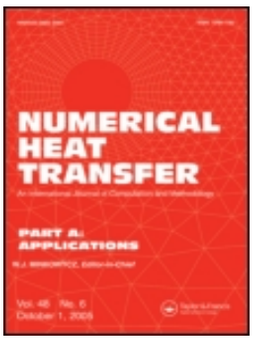

Numerical Heat Transfer, Part A: Applications

ISSN: 1040-7782 (Print) 1521-0634 (Online) Journal homepage: http://www.tandfonline.com/loi/unht20

A Nonequilibrium Finite-Volume Model for Conjugate Fluid/Porous/Solid Domains

Lee Betchen , Anthony G. Straatman & Brian E. Thompson

To cite this article: Lee Betchen , Anthony G. Straatman & Brian E. Thompson (2006) A Nonequilibrium Finite-Volume Model for Conjugate Fluid/Porous/Solid Domains, Numerical Heat Transfer, Part A: Applications, 49:6, 543-565

To link to this article: http://dx.doi.org/10.1080/10407780500430967

Published online: 24 Feb 2007.

Numerical Heat Transfer, Part A, 49: 543–565, 2006

ISSN: 1040-7782 print/1521-0634 online
DOI: 10.1080/10407780500430967

Taylor & Francis
Taylor & Francis Group

A NONEQUILIBRIUM FINITE-VOLUME MODEL FOR CONJUGATE FLUID/POROUS/SOLID DOMAINS

Lee Betchen and Anthony G. Straatman
Department of Mechanical and Materials Engineering, The University of Western Ontario, London, Ontario, Canada

Brian E. Thompson
Department of Mechanical Engineering, The University of Ottawa, Ottawa, Ontario, Canada

A mathematical and numerical model for the treatment of conjugate fluid flow and heat transfer problems in domains containing pure fluid, porous, and pure solid regions is presented. The model is general and physically reasoned, and allows for local thermal nonequilibrium in the porous region. The model is developed for implementation on a simple collocated finite-volume grid. Special attention is given to the matching of the interfacial heat flux, the approximation of advected variables at the interface between pure fluid and porous regions, the pressure–velocity coupling at such an interface, and the estimation of pressure values at the interface.

1. INTRODUCTION

Conjugate fluid flow and heat transfer problems involving domains consisting of pure fluid regions and regions containing saturated porous media are of significant practical importance, finding application in fields such as chemical processing, filtration, metal alloy casting, thermal management, and groundwater flows. In particular, in recent years there has been substantial interest in the use of high-porosity, open-celled metal foams with high thermal conductivity to provide enhanced heat transfer in compact devices. To effectively simulate the performance of such devices, a robust mathematical and numerical model of the fluid flow and heat transfer in a conjugate domain consisting of pure fluid, porous, and pure solid regions is required. Additionally, in the case of air flow through high-conductivity metal foams, where the difference between the fluid and solid constituent thermal conductivities is often two orders of magnitude or more, the assumption of local thermal equilibrium between the two constituents is not generally reasonable [1, 2]. Thus, the case of a two-equation, local thermal nonequilibrium model in the porous region must be considered.

Received 9 February 2005; accepted 30 July 2005.

The authors wish to acknowledge the financial support provided by Oak Ridge National Laboratory, Oak Ridge, TN (USA), and the Ontario Graduate Scholarship (OGS) Program.

Address correspondence to Lee Betchen, The University of Western Ontario, Department of Mechanical and Materials Engineering, London, ON, N6A 5B8, Canada. E-mail: ljbetche@uwo.ca

NOMENCLATURE

a	active coefficient in discretized equation
A	area, m^2
A_{sf}	specific surface area of porous medium, m^{-1}
b	constant coefficient in discretized equation
c	specific heat of a solid, J/kg K
c_E	inertia coefficient of porous medium
c_p	constant-pressure specific heat, J/kg K
d_l	ligament diameter of porous medium, m
d_p	pore diameter of porous medium, m
Da	Darcy number based on channel height ($=K/H^2$)
$\mathbf{f}$	body force per unit mass, m/s^2
$\bar{h}$	overall heat transfer coefficient, $W/m^2 K$
h_{sf}	interfacial heat transfer coefficient in porous medium, $W/m^2 K$
H	channel or block height, m
k	thermal conductivity, W/m K
K	Darcy permeability of porous medium, m^2
L	channel or block length, m
$\mathbf{n}$	outward normal unit vector
Nu	overall Nusselt number ($=\bar{h}L/k_{\text{eff}}$)
Nu_{sf}	interfacial Nusselt number ($=h_{sf}d_l/k_f$)
P	fluid pressure, Pa
Pr	Prandtl number ($=\mu_f c_{p,f}/k_f$)
Pr_{eff}	Effective Prandtl number ($=\mu_f c_{p,f}/k_{\text{eff}}$)
q'	rate of heat transfer per unit depth, W/m
q''	heat flux, W/m^2
Re_{d_l}	Reynolds number based on ligament diameter ($=\rho_f u d_l/\varepsilon\mu_f$)
Re_H	Reynolds number based on channel height ($=\rho_f UH/\mu_f$)
Re_K	Reynolds number based on permeability ($=\rho_f U\sqrt{K}/\mu_f$)
$\mathbf{t}$	tangent unit vector
T	temperature, K
$\mathbf{u}$	fluid velocity [$=(u, v, w) = (u_1, u_2, u_3)$], m/s
$\hat{u}$	advecting velocity, m/s
$\tilde{u}$	pseudo-velocity, m/s
V	volume, m^3
(x, y, z)	Cartesian coordinates $(x, y, z) = (x_1, x_2, x_3)$, m
Δx_{AB}	grid spacing ($=x_B - x_A$), m
δ_{ij}	Kronecker delta function, $\delta_{ij}=1$ if $i=j$, $\delta_{ij}=0$ otherwise
ε	porosity of porous medium
θ	temperature difference
Γ	diffusion coefficient
μ	kinematic viscosity, kg/m s
ρ	density, kg/m^3
$\langle\ \rangle$	denotes averaging

Subscripts and Superscripts

eff	effective property in porous region
f	fluid
fe	effective fluid property in porous region
fl	fluid side of interface
in	inlet
ID	inverse distance approximation
nb	neighbors
o	value at previous time level
P	control volume over which the equation is being integrated
por	porous side of interface
s	solid constituent of porous medium
se	effective solid property in porous region
sol	solid occupying the pure solid region or solid side of interface

Flow in conjugate pure fluid/porous domains has been heavily investigated computationally in recent years, although many of the previous works have been concerned with formulations specific to a particular application. The most prominent such application is the Beavers and Joseph problem, involving fully developed flow in adjacent pure fluid and porous regions with an interface parallel to the direction of flow [3]. Alazmi and Vafai [4] have presented a comprehensive summary of the various models which have been used in consideration of this problem. All of the models considered invoked the assumption of local thermal equilibrium in the

porous region, and the flow was solved directly for fully developed conditions. Alazmi and Vafai [5] have also presented an excellent survey of many of the models currently in use to model the thermal exchange between constituents in the case of local thermal nonequilibrium, however, these are considered in the context of a purely porous domain, rather than a conjugate one. Martins-Costa and Saldanha de Gama [6] have studied this problem for the case of thermal nonequilibrium in the porous region, allowing for accurate solutions to be obtained in situations where the local averaged temperatures in the fluid and solid constituents are expected to be considerably dissimilar. Again, the simplified equations describing fully developed conditions were employed for the fluid flow model.

Many authors have also considered more general implementations of conjugate flow problems, with application to more complex geometries. For example, Chikh et al. [7] have considered the case of a channel with intermittent heated porous blocks mounted on the channel surface, while Fu and Chen [8] considered a similar problem, except allowing for variable porosity within the block. For both cases, the two-dimensional mass-momentum equation set was solved, but local thermal equilibrium was assumed. Ould-Amer et al. [9] considered the case of a channel with solid heat-generating blocks mounted on the surface, and with porous inserts between the blocks, again assuming local thermal equilibrium. The implementation of a nonequilibrium heat transfer model in the presence of an interface with a pure fluid or pure solid region has not often been considered in the open literature, however, such a case was recently examined by Phanikumar and Mahajan [2], who examined the case of natural convection in a conjugate pure fluid/porous domain. In the four general implementations mentioned above, a staggered finite-volume formulation was employed. Though this discretization procedure is straightforward for simple geometries, the staggered grid formulation is more cumbersome in general three-dimensional problems, in particular at interfaces between regions where some volumes overlap and some are adjacent. Recently, Costa et al. [10] have proposed a general control-volume finite-element procedure for the simulation of flows in conjugate pure fluid/porous domains, assuming local thermal equilibrium, in which control volumes centered at the interface are implemented to satisfy the interface conditions implicitly. However, extension of such a method to the case of local thermal nonequilibrium is complicated, and as noted in the validation portion of the present work, the Costa et al. [10] method appears to produce numerical oscillations in the velocity profile near the interface for the case of perpendicular flows at small Darcy number.

The aim of the present work is to develop a robust model and discretization procedure, implemented using the finite-volume method with a simple collocated variable arrangement, which is capable of simulating general fluid flow and heat transfer problems in a conjugate domain consisting of pure fluid, porous, and pure solid regions. Since the method does not require a staggered grid or the location of nodes at the interfaces between regions, the task of generating a suitable grid is simplified, particularly in three-dimensional cases. The model presented here consists of well-established governing equations in each region, including the nonequilibrium heat transfer equations in the porous region. Special attention is given to the development of a physically logical set of conditions to be imposed at the interfaces between regions, and a procedure for discretizing the governing equations and

interface conditions which is effective for a wide range of flow and thermal conditions. In particular, the present model includes physically reasoned estimates for the values of advected variables at the interface between pure fluid and porous regions, for the interfacial conduction heat transfer to or from the fluid and solid constituents of a porous region, and for the pressure at the nominal interface between a pure fluid and porous region.

The mathematical and numerical model described above is presented in this work in a systematic manner. First, the governing equations are presented and discussed for the pure fluid, porous, and pure solid regions. The general interface conditions are then given first for the more complex case of a pure fluid/porous interface, and then for the case of an interface with a pure solid region. Next, the discretization of the governing equations and interface conditions is presented and discussed in the same order as that in which the continuous forms were presented. The model is then validated, with special emphasis placed on demonstrating the validity of key features of the discretization.

2. GOVERNING EQUATIONS

In the present work, the problem under consideration is that of fluid flow and heat transfer in a conjugate domain consisting of pure fluid, porous, and pure solid regions. Figure 1 depicts a respresentative portion of a simple conjugate domain. The mathematical model employed to investigate this situation consists of a set of governing equations for each region, valid in the interior of that region, as well as appropriate conditions to be enforced at the interfaces between regions and the boundaries of the domain.

2.1. Pure Fluid Region

The present work is concerned with the laminar, incompressible flow of a single-phase fluid with constant thermophysical properties. As a result, the fluid flow problem in the pure fluid region is governed by the familiar continuity and Navier–Stokes equations, given respectively as

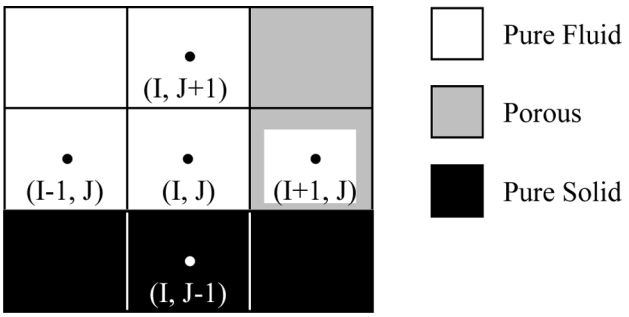

Figure 1. Discretization of an illustrative interface region on a sample two-dimensional structured orthogonal grid.

$$\rho_f(\nabla \cdot \mathbf{u}) = 0 \tag{1}$$

$$\rho_f\left[\frac{\partial \mathbf{u}}{\partial t} + \nabla \cdot (\mathbf{uu})\right] = -\nabla P + \mu_f \nabla^2 \mathbf{u} + \rho_f \mathbf{f} \tag{2}$$

Under the additional assumption that the effects of viscous dissipation and heat generation may be neglected, the heat transfer portion of the problem is governed by the following form of the energy equation:

$$\rho_f c_{p,f}\left[\frac{\partial T}{\partial t} + \nabla \cdot (\mathbf{u}T)\right] = k_f \nabla^2 T \tag{3}$$

2.2. Porous Region

In the porous region, the well-known local volume-averaged forms of the governing equations are used. At this juncture, it is useful to define three distinct types of averaging, which will be referred to in this work. The extrinsic, or superficial, average of a property φ_i associated with constituent i is defined as

$$\langle \varphi_i \rangle = \frac{1}{V}\int_{V_i} \varphi_i \, dV \tag{4}$$

where V is a representative elementary volume containing both fluid and solid constituents, and V_i is the volume of constituent i located within V [11]. The intrinsic average is defined as

$$\langle \varphi_i \rangle^i = \frac{1}{V_i}\int_{V_i} \varphi_i \, dV \tag{5}$$

As can be seen from Eq. (5), the intrinsic average is the true average value of φ_i in constituent i over the volume V. Clearly, since $\varepsilon = V_f/V$, we may employ the relation $\langle \varphi \rangle = \varepsilon \langle \varphi_f \rangle^f$. Finally, the total average over V of a property φ defined in both the fluid and solid constituents is given by

$$\langle \varphi \rangle = \frac{1}{V}\int_V \varphi dV \tag{6}$$

Then, taking the extrinsic average of Eq. (1), the volume-averaged continuity equation may be expressed in the form [12, 13]

$$\rho_f(\nabla \cdot \langle \mathbf{u} \rangle) = 0 \tag{7}$$

Subject to appropriate length-scale constraints, the volume-averaged momentum equations are typically expressed in intrinsic form, representing a force balance per unit volume of the fluid constituent [12]. Assuming a constant porosity, this

leads to [12, 13]

$$\frac{\rho_f}{\varepsilon}\frac{\partial\langle\mathbf{u}\rangle}{\partial t}+\frac{\rho_f}{\varepsilon^2}\nabla\cdot(\langle\mathbf{u}\rangle\langle\mathbf{u}\rangle)=-\nabla\langle P\rangle^f+\frac{\mu_f}{\varepsilon}\nabla^2\langle\mathbf{u}\rangle-\frac{\mu_f}{K}\langle\mathbf{u}\rangle - \frac{\rho_f C_E}{\sqrt{K}}|\langle\mathbf{u}\rangle|\langle\mathbf{u}\rangle+\rho_f\mathbf{f} \tag{8}$$

where the familiar Darcy and Forchheimer terms have been used heuristically to close the set of equations, replacing respectively the information regarding the viscous and form drag interaction between the fluid and solid constituents which is lost in volume averaging the velocity field. The second term on the right-hand side of Eq. (8) represents the macroscopic viscous effects, and is historically referred to as the Brinkman term. For the purposes of this work, the extrinsic form of Eq. (8) is more desirable, and is found to be [12]

$$\rho_f\frac{\partial\langle\mathbf{u}\rangle}{\partial t}+\frac{\rho_f}{\varepsilon}\nabla\cdot(\langle\mathbf{u}\rangle\langle\mathbf{u}\rangle)=-\varepsilon\nabla\langle P\rangle^f+\mu_f\nabla^2\langle\mathbf{u}\rangle-\frac{\varepsilon\mu_f}{K}\langle\mathbf{u}\rangle - \frac{\varepsilon\rho_f c_E}{\sqrt{K}}|\langle\mathbf{u}\rangle|\langle\mathbf{u}\rangle+\varepsilon\rho_f\mathbf{f} \tag{9}$$

As discussed above, in the interest of generality, the heat transfer problem in the porous region will be treated under the assumption of local thermal nonequilibrium, that is, we will not assume that $\langle T_f\rangle^f=\langle T_s\rangle^s=\langle T\rangle$ at a given point. This gives rise to extrinsic volume-averaged energy equations of the form [14]

$$\rho_f c_{p,f}\left[\varepsilon\frac{\partial\langle T_f\rangle^f}{\partial t}+\nabla\cdot\left(\langle\mathbf{u}\rangle\langle T_f\rangle^f\right)\right]=k_{fe}\nabla^2\langle T_f\rangle^f+h_{sf}A_{sf}\left(\langle T_s\rangle^s-\langle T_f\rangle^f\right) \tag{10}$$

$$(1-\varepsilon)\rho_s c_s\frac{\partial\langle T_s\rangle^s}{\partial t}=k_{se}\nabla^2\langle T_s\rangle^s-h_{sf}A_{sf}\left(\langle T_s\rangle^s-\langle T_f\rangle^f\right) \tag{11}$$

for the fluid and solid constituents, respectively. Note that in Eq. (10), the fluid-phase effective thermal conductivity k_{fe} may include a component accounting for the effects of thermal dispersion. The stagnant portions of the effective conductivity are typically obtained by developing a model for the total effective conductivity based on a simplified model of the pore geometry. Then, by taking the fluid constituent conductivity to be the appropriate value and setting the solid constituent conductivity to zero, such a model yields the value of k_{fe}. The solid constituent effective conductivity k_{se} is obtained in a similar manner. The most common such model [11] is the simple estimate $k_{fe}=\varepsilon k_f$ and $k_{se}=(1-\varepsilon)k_s$, however, this model tends to overestimate the conductivities of many materials. Here, in the interest of generality, we do not specify a particular model, though for the nonequilibrium heat transfer test case, the model of Calmidi and Mahajan [1] is employed. The second term on the right-hand side of Eqs. (10) and (11) represents the heat transfer between the fluid and solid constituents.

2.3. Pure Solid Region

In the pure solid region, the heat transfer problem is governed by the familiar conduction equation, again neglecting the effects of heat generation:

$$\rho_{\text{sol}} c_{\text{sol}} \frac{\partial T}{\partial t} = k_{\text{sol}} \nabla^2 T \tag{12}$$

3. INTERFACE CONDITIONS

3.1. Interface between Pure Fluid and Porous Regions

Appropriate conditions for the fluid flow problem at the interface between a pure fluid region and a porous region have been extensively studied in the open literature in recent years [2, 4, 6, 10, 11, 15–19]. In this work, the physically reasonable condition of continuity of the velocity at the interface is enforced, that is,

$$\mathbf{u}_{fl} = \langle \mathbf{u} \rangle_{\text{por}} \tag{13}$$

Obviously, the velocity $\mathbf{u}$ on the pure fluid side immediately at the nominal interface is not strictly the point velocity but rather an average value, although the two quickly become equivalent away from the interface [17]. The same reasoning holds for all other distributions in the fluid or solid regions near the interface. Additionally, we enforce continuity of the interfacial stress on the pure fluid side with the intrinsically averaged stress on the porous side, leading to the conditions [6, 18, 19]

$$\begin{aligned} (\mathbf{n} \cdot \mathbf{t} \cdot \sigma)_{fl} &= \left(\mathbf{n} \cdot \mathbf{t} \cdot \langle \sigma \rangle^f \right)_{\text{por}} \qquad \text{(shear stress)} \\ (\mathbf{n} \cdot \mathbf{n} \cdot \sigma)_{fl} &= (\mathbf{n} \cdot \mathbf{n} \cdot \langle \sigma \rangle^f)_{\text{por}} \qquad \text{(normal stress)} \end{aligned} \tag{14}$$

where the stress tensors in Eqs. (14) are given by

$$\begin{aligned} \sigma_{ij} &= \mu_f \left(\frac{\partial u_i}{\partial x_j} + \frac{\partial u_j}{\partial x_i} \right) - P \delta_{ij} \\ \langle \sigma_{ij} \rangle^f &= \frac{\mu_f}{\varepsilon} \left(\frac{\partial \langle u_i \rangle}{\partial x_j} + \frac{\partial \langle u_j \rangle}{\partial x_i} \right) - \langle P \rangle^f \delta_{ij} \end{aligned} \tag{15}$$

where δ_{ij} is the typical Kronecker delta function. Physically, from the form of Eq. (9), Eqs. (14) imply that a fraction ε of the total stress on the pure fluid side of the interface is carried in the fluid constituent of the porous medium, with the remainder carried by the solid constituent [18]. Finally, we will insist that the pressure on the pure fluid side of the interface be continuous with the intrinsically averaged pressure on the porous side, that is,

$$P_{\text{fl}} = \langle P \rangle^f_{\text{por}} \tag{16}$$

Note that since the portion of the interface normal stress due to pressure is continuous, from Eqs. (14)–(15) we have also that the viscous portion of the normal stress is continuous. Although we enforce the condition of Eq. (16) in the sense that we use

a single value for the pressure at the nominal interface $P_{\mathrm{fl}} = \langle P \rangle^{f}_{\mathrm{por}}$, it is clear from the differing forms of the advected velocity in Eqs. (2) and (9) that we must in general allow for a rapid change in pressure to occur in pure fluid region near the interface, associated with the dynamic pressure effects.

For the heat transfer problem, the temperature on the pure fluid side of the interface is taken to be continuous with the total average temperature on the porous side for thermal equilibrium of the interface [2, 6]. Based on this requirement and an energy balance on the interface, the interface conditions are found to be

$$\begin{aligned} T_{\mathrm{fl}} = \langle T \rangle_{\mathrm{por}} &= \left(\varepsilon \langle T_f \rangle^{f} + (1-\varepsilon) \langle T_s \rangle^{s} \right)_{\mathrm{por}} \\ \left(-k_f \frac{\partial T}{\partial n} \right)_{\mathrm{fl}} &= \left(-k_{\mathrm{fe}} \frac{\partial \langle T_f \rangle^{f}}{\partial n} - k_{\mathrm{se}} \frac{\partial \langle T_s \rangle^{s}}{\partial n} \right)_{\mathrm{por}} \end{aligned} \tag{17}$$

3.2. Interfaces with Pure Solid Region

The conditions to be enforced on the velocity and pressure fields at an interface with a pure solid region are well known and are identical to the conditions typically enforced at an impermeable boundary. The typical no-slip and no-penetration conditions are employed for the velocity at the interface, while the pressure at the interface is simply obtained by extrapolation from the interior of the region. These conditions apply equally to interfaces with a fluid region or a porous region.

The conditions for the heat transfer problem at an interface between pure fluid and pure solid regions are fairly straightforward. From the continuity of the temperature distribution and an energy balance on the interface, these conditions are given as

$$\begin{aligned} T_{\mathrm{sol}} &= T_{\mathrm{fl}} \\ \left(-k_{\mathrm{sol}} \frac{\partial T}{\partial n} \right)_{\mathrm{sol}} &= \left(-k_f \frac{\partial T}{\partial n} \right)_{\mathrm{fl}} \end{aligned} \tag{18}$$

Similarly to Eq. (17), the conditions employed at an interface between pure solid and porous regions are of the form

$$\begin{aligned} T_{\mathrm{sol}} &= \langle T \rangle_{\mathrm{por}} \\ \left(-k_{\mathrm{sol}} \frac{\partial T}{\partial n} \right)_{\mathrm{sol}} &= \left(-k_{\mathrm{fe}} \frac{\partial \langle T_f \rangle^{f}}{\partial n} - k_{\mathrm{se}} \frac{\partial \langle T_s \rangle^{s}}{\partial n} \right)_{\mathrm{por}} \end{aligned} \tag{19}$$

4. DISCRETIZATION AND IMPLEMENTATION

In this section, the discretized forms of the model equations for the heat transfer and fluid flow problems in conjugate domain are presented. The discrete equations are given fully so that modifications required at the domain interfaces can be clearly identified. The discretized governing equations for the interiors of each region are presented first, followed by the discretized interface conditions.

4.1. Governing Equations

In order to obtain the discretized form of the governing equations outlined above for solution in a collocated finite-volume framework, these equations must be integrated over a typical control volume. Considering a volume V bounded by N faces and centered about a node P, the partially discretized forms of Eqs. (1)–(3) are given respectively for a fully implicit discretization as [20]

$$\sum_i \dot{m}_i = 0 \tag{20}$$

$$\frac{\rho_f V_P(\mathbf{u}_P - \mathbf{u}_P^o)}{\Delta t} + \sum_i \dot{m}_i(\mathbf{u}_i - \mathbf{u}_P) = -V_P(\nabla P)_P + \sum_i \mu_f \left(A \frac{\partial \mathbf{u}}{\partial \boldsymbol{n}} \right)_i + \rho_f V_P \mathbf{f}_P \tag{21}$$

$$\frac{\rho_f V_P c_{p,f}(T_P - T_P^o)}{\Delta t} + \sum_i \dot{m}_i c_{p,f}(T_i - T_P) = \sum_i k_f \left(A \frac{\partial T}{\partial n} \right)_i \tag{22}$$

In Eqs. (20)–(22), terms with the subscript i, $i = 1, 2, \ldots, N$, are evaluated at the integration point lying at the centroid of face i. Note that Eq. (21) is actually obtained by subtracting Eq. (20), multiplied by $\mathbf{u}_P$, from the discretized form of Eq. (2), and similarly for Eq. (22). This is done to ensure a conservative method. The values of the advected properties $\mathbf{u}_i$ and T_i may be determined in the interior of the region from any convenient numerical scheme, as may the face temperature and velocity gradients and the cell-centered pressure gradient. The mass flow rate is given by

$$\dot{m}_i = \rho_f A_i(\widehat{\mathbf{u}}_i \cdot \mathbf{n}) \tag{23}$$

where the advecting velocity $\widehat{\mathbf{u}}_i \cdot \mathbf{n}$ is found in accordance with the collocated variable method of Rhie and Chow [21]. As an example, designate node $(I, J-1)$ of the simple grid illustrated in Figure 1 as the P node in the standard terminology, and consider the advecting velocity $\widehat{u}_e$ at the integration point e located on the east face of the volume associated with that node. First, it must be noticed that upon insertion of appropriate approximations for the face velocity gradients and advected velocities, the component of Eq. (21) in the x direction may be written as [20]

$$a_P u_P = \sum_{\text{nb}} a_{\text{nb}} u_{\text{nb}} + b_P - V_P \left. \frac{\partial P}{\partial x} \right|_P = \widetilde{u}_P - V_P \left. \frac{\partial P}{\partial x} \right|_P \tag{24}$$

A similar equation also holds at the E node (I, J). Then, an estimate for $\widehat{u}_e$ is sought by constructing an approximate momentum equation in the form of Eq. (24) about the integration point e. That is, we seek to estimate $\widehat{u}_e$ in the form

$$\widehat{u}_e = \frac{\widetilde{u}_e}{a_e} - \left. \frac{V_e}{a_e} \frac{\partial P}{\partial x} \right|_e \tag{25}$$

The approximations $a_e \approx (a_P + a_E)/2$ and $V_e \approx (V_P + V_E)/2$ are employed, and $\widetilde{u}_e$ is approximated from an inverse distance average of the values at P and E, making use of the further simplifications $a_e \approx a_P \approx a_E$ and $V_e \approx V_P \approx V_E$. Note that here,

a_E is the active coefficient for the node (I, J) in its own momentum equation. Finally, this leads to

$$\widehat{u}_e = u_e^{\mathrm{ID}} - \frac{V_e}{a_e}\left(\left.\frac{\partial P}{\partial x}\right|_e - \left.\frac{\partial P}{\partial x}\right|_e^{\mathrm{ID}}\right) \tag{26}$$

The first pressure gradient term in Eq. (26) is an approximation based of the values surrounding the e integration point and is treated implicitly in Eq. (20), while the second is the inverse distance approximation based on the cell-centered values at P and E and is deferred.

The discretization of Eqs. (7), (9), (10), and (11) for the porous region proceeds in a manner exactly similar to that for the discretization process in porous media. The discretized forms of these equations may readily be found as, respectively,

$$\sum_i \dot{m}_i = 0 \tag{27}$$

$$\begin{aligned}\frac{\rho_f V_P(\langle \mathbf{u}\rangle_P - \langle \mathbf{u}\rangle_P^o)}{\Delta t} + \sum_i \dot{m}_i\left(\frac{\langle \mathbf{u}\rangle_i}{\varepsilon} - \frac{\langle \mathbf{u}\rangle_P}{\varepsilon}\right)\\ = -\varepsilon V_P\left(\nabla\langle P\rangle^f\right)_P + \sum_i \mu_f\left(A\frac{\partial\langle \mathbf{u}\rangle}{\partial n}\right)_i - \frac{\varepsilon V_P \mu_f}{K}\langle \mathbf{u}\rangle_P\\ - \frac{\varepsilon\rho_f V_P c_E}{\sqrt{K}}\left|\langle \mathbf{u}\rangle_P\right|\langle \mathbf{u}\rangle_P + \rho_f V_P \mathbf{f}_P\end{aligned} \tag{28}$$

$$\begin{aligned}\frac{\varepsilon\rho_f V_P c_{p,f}\left(\langle T_f\rangle_P^f - \langle T_f\rangle_P^{f,o}\right)}{\Delta t} + \sum_i \dot{m}_i c_{p,f}\left(\langle T_f\rangle_i^f - \langle T_f\rangle_P^f\right)\\ = \sum_i k_{\mathrm{fe}}\left(A\frac{\partial\langle T_f\rangle^f}{\partial n}\right)_i + h_{sf}A_{sf}V_P\left(\langle T_s\rangle_P^s - \langle T_f\rangle_P^f\right)\end{aligned} \tag{29}$$

$$\frac{(1-\varepsilon)\rho_s V_P c_s\left(\langle T_s\rangle_P^s - \langle T_s\rangle_P^{s,o}\right)}{\Delta t} = \sum_i k_{\mathrm{se}}\left(A\frac{\partial\langle T_s\rangle^s}{\partial n}\right)_i - h_{sf}A_{sf}V_P\left(\langle T_s\rangle_P^s - \langle T_f\rangle_P^f\right) \tag{30}$$

Again, the mass flow rate is of the form of Eq. (23), with $\widehat{\mathbf{u}}_i$ replaced by $\langle\widehat{\mathbf{u}}\rangle_i$. The approximation for the advecting velocity is obtained based on precisely the same reasoning used to arrive at Eq. (26), noting that Eq. (24) is replaced by the slightly

different form

$$a_P\langle u\rangle_P=\langle\widetilde{u}\rangle_P-\varepsilon V_P\left.\frac{\partial\langle P\rangle^f}{\partial x}\right|_P \tag{31}$$

Considering as an example the advecting velocity $\langle\widehat{u}\rangle_e$ at the integration point e associated with the volume $(I+1, J)$ of Figure 1, the approximation may be simply seen to be

$$\langle\widehat{u}\rangle_e=\langle u\rangle_e^{\mathrm{ID}}-\frac{\varepsilon V_e}{a_e}\left(\left.\frac{\partial\langle P\rangle^f}{\partial x}\right|_e-\left.\frac{\partial\langle P\rangle^f}{\partial x}\right|_e^{\mathrm{ID}}\right) \tag{32}$$

where the same definitions of apply to Eq. (31) as Eq. (26).

Finally, in the pure solid region, only a discretized energy equation is required. Integrating Eq. (12), the appropriate form of the energy equation is [20]

$$\frac{\rho_{\mathrm{sol}}V_Pc_{\mathrm{sol}}(T_P-T_P^o)}{\Delta t}=\sum_i k_{\mathrm{sol}}\left(A\frac{\partial T}{\partial n}\right)_i \tag{33}$$

4.2. Interface between Pure Fluid and Porous Regions

To obtain accurate estimates of the terms in the discretized governing equations for volumes adjacent to an interface, the interface conditions given above are employed. First, it should be noted that on a volume immediately on the fluid side of an interface between pure fluid and porous regions, a modification must be made to the advective terms in Eqs. (21) and (22). Physically, the discretized advective momentum and energy transfer terms should be continuous at a face which coincides with a pure fluid/porous interface, and it is must be the intrinsic fluid velocity and temperature that are advected. Then, considering the example of the volume (I, J) of Figure 1, the discretized advective momentum and energy transfer corresponding to the east-face integration point e of that volume should be given respectively as $\dot{m}_e\langle\mathbf{u}\rangle_e/\varepsilon$ and $\dot{m}_ec_{p,f}\langle T_f\rangle_e^f$. The form of the advected velocity may be understood by idealizing the interface as an array of a large number of sudden expansions or contractions, depending on flow direction, where ε may be interpreted as the ration of the cross-sectional flow area on the porous side of the interface to that on the pure fluid side. Obviously, the energy advected by the flow at the interface should be expressed in terms of the intrinsic temperature of the fluid at that location. Following is the development of suitable approximations for the relevant terms.

Advecting velocities. A control-volume face coinciding with a pure fluid/porous interface presents a special case in terms of the formulation of the advecting velocity. Again, an estimate is sought for the advecting velocity based on the formulation of an approximate momentum equation about the face. Considering the advecting velocity $\langle\widehat{u}\rangle_e=\widehat{u}_e$ at the east face of the volume (I, J) of Figure 1, the form of the momentum equation is that of Eq. (24) for the P node, and that of Eq. (31) for the E node. Then, an approximate momentum equation is formulated for the volume $V_e=(V_P+V_E)/2$, introducing the assumptions $a_e\approx(a_P+a_E)/2$ and

$\langle \widetilde{u} \rangle_e \approx (\widetilde{u}_P + \langle \widetilde{u} \rangle_E)/2$, leading to an estimate of the form

$$\langle \widehat{u} \rangle_e = \frac{1}{2}\left(\frac{a_P}{a_e} u_P + \frac{a_E}{a_e}\langle u \rangle_E\right) - \frac{V_e}{a_e}\left[\overline{\left(\frac{\partial P}{\partial x}\right)}\bigg|_e - \frac{1}{2}\left(\frac{V_P}{V_e}\frac{\partial P}{\partial x}\bigg|_{P+} + \frac{\varepsilon V_E}{V_e}\frac{\partial \langle P \rangle^f}{\partial x}\bigg|_{E-}\right)\right]$$

$$\overline{\left(\frac{\partial P}{\partial x}\right)}\bigg|_e = \frac{1}{V_e}\left(\frac{V_P}{2}\frac{\partial P}{\partial x}\bigg|_{P+} + \frac{\varepsilon V_E}{2}\frac{\partial \langle P \rangle^f}{\partial x}\bigg|_{E-}\right) \tag{34}$$

Note that at the interface, the assumption $a_e \approx a_P \approx a_E$ is not made, since obviously a_P and a_E may be substantially different due to the potentially large source terms present in Eq. (28). Note also that in Eq. (34), the subscript $P+$ denotes the average value between P and e, and similarly $E-$ denotes an average between e and E. As will be seen when the approximation for the interface pressure is developed, the use of estimates to the pressure gradient over only half of the volume in calculating the advecting velocities at the faces of volumes adjacent to the interface is important, since the behavior over the two halves of the volume may be substantially different. Also, analogously with Eq. (26), the second and third pressure gradient terms in the first of Eqs. (34) are deferred. That a slightly different methodology is used to arrive at Eqs. (34), in comparison to Eqs. (26) and (32), is a result of the generally discontinuous nature of the pressure gradient at the interface, and the substantial differences between the momentum equations of either side of the interface. The development of Eqs. (34) reflects a physically realistic approximation to a momentum balance over a control volume containing the east half of V_P and the west half of V_E, and Eqs. (34) have been found by the authors to be necessary for maintaining a strong coupling of pressure and velocity.

Diffusive and advective terms. From Eqs. (22) and (28), it is seen that only the portions of the viscous stresses involving the face-normal components of the gradients of the velocity components appear explicitly in the formulation of the governing equations for an incompressible fluid. Then, for ease of implementation, we modify slightly the conditions of Eq. (14) to require that these portions of the viscous stress balance individually on either side of the interface, that is,

$$\mu_f\left(\frac{\partial \mathbf{u}}{\partial n}\right)_{\mathrm{fl}} = \frac{\mu_f}{\varepsilon}\left(\frac{\partial \langle \mathbf{u} \rangle}{\partial n}\right)_{\mathrm{por}} \tag{35}$$

Considering again the example of the east face of volume (I, J) in Figure 1, it is clear that Eqs. (14)–(16) and Eq. (35) place the requirements on the normal stress at the interface, but that the shear stress conditions differ:

$$\begin{aligned} \mu_f\left(\frac{\partial u}{\partial y} + \frac{\partial v}{\partial x}\right)_{\mathrm{fl}} &= \frac{\mu_f}{\varepsilon}\left(\frac{\partial \langle u \rangle}{\partial y} + \frac{\partial \langle v \rangle}{\partial x}\right)_{\mathrm{por}} && \text{[Eq. (14)]} \\ \mu_f\left(\frac{\partial v}{\partial x}\right)_{\mathrm{fl}} &= \frac{\mu_f}{\varepsilon}\left(\frac{\partial \langle v \rangle}{\partial x}\right)_{\mathrm{por}} && \text{[Eq. (35)]} \end{aligned} \tag{36}$$

Now, a method of approximating the viscous terms based on the requirements of Eqs. (13) and (35) is needed. First, consider a more general diffusive balance for

an independent variable continuous at the interface between two regions of the form

$$\Gamma_1 \left(\frac{\partial \phi}{\partial n}\right)_1 = \Gamma_2 \left(\frac{\partial \phi}{\partial n}\right)_2 \tag{37}$$

where Γ_1 and Γ_2 are diffusion coefficients. Using one-sided estimates to the derivatives at the interface, the requirement of Eq. (37) may be discretized for the east face of volume (I, J) as follows:

$$\Gamma_1 \frac{\phi_e - \phi_P}{\Delta x_{Pe}} = \Gamma_2 \frac{\phi_E - \phi_e}{\Delta x_{eE}} \tag{38}$$

An estimate for the interface value of the dependent variable ϕ is found in the form

$$\phi_e = \left(1 + \frac{\Gamma_2}{\Gamma_1}\frac{\Delta x_{Pe}}{\Delta x_{eE}}\right)^{-1} \phi_P + \left(1 + \frac{\Gamma_1}{\Gamma_2}\frac{\Delta x_{eE}}{\Delta x_{Pe}}\right)^{-1} \phi_E \tag{39}$$

Inserting Eq. (39) on both sides of Eq. (38), the estimate to the diffusive flux is given as

$$\Gamma_1 \left(\frac{\partial \phi}{\partial n}\right)_1 = \Gamma_2 \left(\frac{\partial \phi}{\partial n}\right)_2 \approx \frac{\phi_E - \phi_P}{((\Delta x_{Pe}/\Gamma_1) + (\Delta x_{eE}/\Gamma_2))} \tag{40}$$

Note that Eq. (40) is the harmonic mean formulation of Patankar [20]. This formulation is used to approximate the terms of Eq. (35) for the east face of volume (I, J) as

$$\mu_f \left(\frac{\partial \mathbf{u}}{\partial n}\right)_{\text{fl}} = \frac{\mu_f}{\varepsilon}\left(\frac{\partial \langle \mathbf{u} \rangle}{\partial n}\right)_{\text{por}} \approx \mu_f \frac{\langle \mathbf{u} \rangle_E - \mathbf{u}_P}{\Delta x_{Pe} + \varepsilon \Delta x_{eE}} \tag{41}$$

Note, however, that the viscous flux at the west face of volume $(I+1, J)$ is, according to Eq. (28), only a fraction ε of the result of Eq. (41). As mentioned above, this is because only part of the interface stress is carried by the fluid constituent of the porous medium, with the remainder carried by the solid constituent. This formulation also provides a convenient and physically based estimate of the advective momentum transfer at the interface, with $\langle \mathbf{u} \rangle_e$ estimated readily by Eq. (39). This approximation has been implemented by the authors using a deferred correction scheme, and is employed in all test cases presented in this work.

The conditions required to match the energy equation in the pure fluid region to the two nonequilibrium equations in the porous region have not been heavily investigated [2, 6]. Although it is clear that an energy balance must exist at the interface as per the second of Eqs. (7), what is not obvious is how the total heat conducted into or out of the interface on the pure fluid side is distributed between the fluid and solid constituents on the porous side. Some investigators have suggested a uniform distribution based on surface area fraction [6]. However, when dealing with a solid constituent of extremely high thermal conductivity, this approximation is somewhat unsatisfying. In such a case, one physically would expect that the conduction heat transfer to or from the solid constituent could indeed be greater than that of the fluid constituent, even if the porosity is relatively high. To allow for this, we relax slightly the common idealization of the interface effects as essentially one-dimensional,

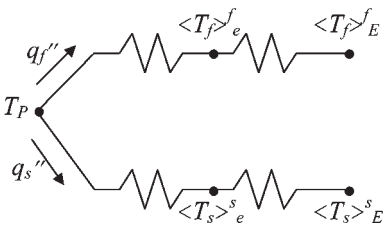

Figure 2. Thermal resistance network for development of parallel model for interface conduction.

modeling the conduction between the pure fluid region and the fluid and solid constituents of the porous medium as a parallel conduction process. The thermal circuit for this model is illustrated in Figure 2 for the heat transfer across the east face of volume (I, J) in Figure 1. This leads to discrete energy balances of the form

$$\begin{aligned} q_f'' &= \varepsilon k_f \frac{\langle T_f \rangle_e^f - T_P}{\Delta x_{Pe}} = k_{fe} \frac{\langle T_f \rangle_E^f - \langle T_f \rangle_e^f}{\Delta x_{eE}} \\ q_s'' &= (1-\varepsilon) k_f \frac{\langle T_s \rangle_e^s - T_P}{\Delta x_{Pe}} = k_{se} \frac{\langle T_s \rangle_E^s - \langle T_s \rangle_e^s}{\Delta x_{eE}} \end{aligned} \tag{42}$$

The sum of both of Eqs. (42) gives the total heat flux for use in the pure fluid energy equation. Note that Eqs. (42) still satisfy the thermal equilibrium requirement of the first of Eqs. (17) in an average sense, as well as satisfying the energy balance. Obviously, Eqs. (42) each have the form of Eq. (38) and may be easily implemented using Eq. (40). The use of the first of Eqs. (42) in conjunction with Eq. (39) provides a physical estimate to the advected temperature at the interface. Note also that though this particular problem is not well studied, Alazmi and Vafai [22] have thoroughly considered the similar problem of the division of a constant wall heat flux between the two constituents of a porous medium under the conditions of thermal nonequilibrium. The model at which we have arrived here is based on a principle similar to many of the models presented in that work.

Interface pressure. In order to estimate the average pressure gradient terms appearing in Eqs. (21), (28), and (34), an approximation to the pressure at the interface must be determined. However, the pressure gradient at the interface is not generally expected to be continuous, as a result of the rather large Darcy and Forchheimer terms present on the porous side, which represent essentially a momentum sink, so that the typical approximations for pure fluid flows may not be terribly accurate. This task is complicated by the fact that, as described above, the advected velocity changes rapidly in the vicinity of the interface. In order to derive a suitable estimate to the pressure at the interface, consider the simple grid of Figure 3, and the control volume illustrated by the dotted lines, whose east face is coincident with the interface. Assume that the horizontal extent δ of the control volume is an indeterminate small distance much less than the height of the control volume, and much less than the distance Δx_{Pe}, but large enough so that the advected velocity at the west face is not yet affected by the abrupt change in flow area at the interface. Then,

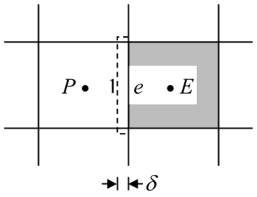

Figure 3. Control volume for development of interface pressure estimate.

the momentum flux from the surfaces normal to the vertical direction may be neglected, the viscous stresses may be assumed to balance separately, and the advected velocity at the west face may be assumed to be $u_1 \approx u_e = \langle u \rangle_e$. Then, a momentum balance on the control volume yields

$$\langle P \rangle_e^f = P_e \approx P_1 - \frac{\dot{m}_e \langle u \rangle_e}{A_e} \frac{1-\varepsilon}{\varepsilon} \tag{43}$$

or, for an arbitrarily oriented interface i,

$$\langle P \rangle_i^f = P_i \approx P_1 - \frac{\dot{m}_i \langle \mathbf{u} \rangle_i \cdot \mathbf{n}}{A_i} \frac{1-\varepsilon}{\varepsilon} \tag{44}$$

Assuming that location 1 is nearly coincident with the interface due to the assumption $\delta << \Delta x_{Pe}$, and, assuming that similar conditions prevail over the majority of the control volume, an estimate of P_1 may be obtained from simple extrapolation to the interface from the interior of the pure fluid region. Then, Eq. (44) constitutes an estimate to the interface pressure based on the conditions in the pure fluid region. This estimate is then averaged with an estimate based on the conditions in the porous region, obtained directly from extrapolation, to arrive at the final estimate to the interface pressure. In the authors' structured code, a second-order Taylor series estimate is used for the extrapolations. Note that the estimate to the interface pressure obtained from the above arguments, though physically reasoned, is somewhat complex and thus is best implemented in a deferred fashion, with a simpler estimate, such as straightforward inverse distancing, implemented implicitly. Finally, notice that the estimate of the interface pressure depends on the mass flow rate at the interface, which in turn depends on the interface pressure as a consequence of the form of the advecting velocity. Then, at the end of each iteration of the linearization loop, when new values of the interface pressure and mass flow rate are calculated based on the most recent pressure and velocity field, a small number of iterations is required to ensure accuracy.

4.3. Interfaces with Pure Solid Region

The discretization of the conditions for the fluid flow problem at an interface between a pure fluid or porous region, and a solid region, are straightforward and identical to the implementation of boundary conditions at an impermeable boundary. The conduction heat flux at the interface between a pure solid and a pure fluid region may be simply discretized using Eq. (40) to implement the conditions of

Eqs. (18). Based on the same argument outlined above for a pure fluid/porous interface, the conduction heat flux at a pure solid/porous interface may be discretized using the parallel conduction model, yielding a set of equations identical in form to Eqs. (42), and the model may again be implemented using Eq. (40).

5. VALIDATION

Test cases are conducted to demonstrate the accuracy and utility of the conjugate formulation presented in the previous sections. The Beavers-Joseph problem is solved to illustrate the accuracy of the formulation in comparison to previous published work. A porous plug flow is then solved to illustrate the robustness of the interface conditions and modified coupling schemes over a range of Reynolds numbers. Finally, a documented heat transfer problem is solved to illustrate the utility of the nonequilibrium thermal model.

5.1. Beavers and Joseph Problem

The Beavers and Joseph problem is a well-known case of steady plane flow in the presence of an interface between pure fluid and porous regions which is parallel to the flow direction. This case was originally considered experimentally by Beavers and Joseph [3], and as previously mentioned, has been heavily investigated computationally. Thus, it is a logical test case to evaluate the accuracy of the present method in the case of a parallel interface. Although Beavers and Joseph originally considered the case of a semi-infinite porous domain, for simplicity we follow Costa et al. [10] and Gartling et al. [15] in slightly modifying the problem to the geometry illustrated in Figure 4. This problems was considered for the conditions $\mathrm{Re}_H = 1$, $\varepsilon = 0.7$, and Darcy numbers Da of 10^{-2} and 10^{-3}, with the inertia coefficient given by the familiar relation $c_E = 1.75\varepsilon/(150\varepsilon^5)^{1/2}$. Note that the Reynolds number $\mathrm{Re}_H = \rho_f UH/\mu_f$, where U is the average velocity in the pure fluid portion of the channel at fully developed conditions. To test the implementation more rigorously, a uniform velocity distribution was specified at the inlet of the channel and the flow was allowed to develop, as opposed to simulating the fully developed flow directly using cyclic boundary conditions. A channel length of $L = 8H$ was selected to ensure a fully developed profile at the outlet. Then, the boundary conditions imposed on the velocity profile, with reference to Figure 4, were the uniform inlet velocity

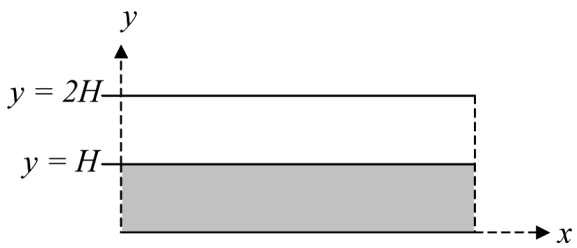

Figure 4. Geometry of modified Beavers and Joseph problem.

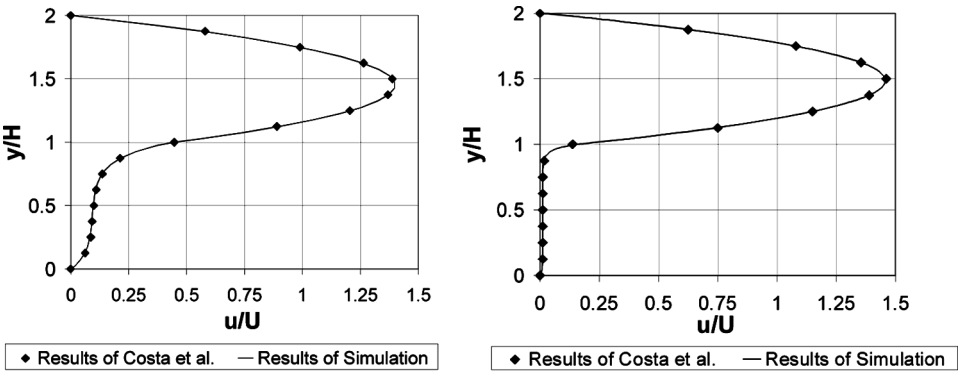

Figure 5. Fully developed velocity profile for Beavers and Joseph problem with $\mathrm{Re} = 1$, $c_E = 1.75\varepsilon/(150\varepsilon^5)^{1/2}$, $\varepsilon = 0.7$, and (*a*) $\mathrm{Da} = 10^{-2}$, (*b*) $\mathrm{Da} = 10^{-3}$.

distribution $u(0, y) = U_0$ and $v(0, y) = 0$, where U_0 was chosen to provide the desired Reynolds number at fully developed conditions, zero derivative conditions in the x direction on both velocities at $x = L$, and the typical conditions $u = v = 0$ at $y = 0$ and $y = 2H$. A uniform pressure condition was set at $x = L$, and extrapolated pressure conditions were employed at all other boundaries. After a careful grid convergence study, a structured grid consisting of 40 volumes in the y direction and 100 volumes in the x direction was selected. The grid was slightly refined toward the inlet, and also toward the interface for the case of $\mathrm{Da} = 10^{-3}$. For all validation cases presented in this section, the advection scheme used in the interior of each domain was the typical first-order Peclet-weighted upwind differencing, and the normalized residuals for the discrete, linearized governing equations were reduced to below the value 10^{-6} for each control volume.

The fully developed velocity profiles obtained from the present formulation are shown in Figure 5, with the results of Costa et al. [10] given for comparison. Note that although the modeled momentum equations employed in the porous region by Costa et al. are slightly different than those used here, the difference should not affect the results of this problem since the difference occurs in the form of the macroscopic convective term, which is identically zero under fully developed conditions. The results obtained in the present study are seen be nearly identical to those of Costa et al. for both Darcy numbers considered, demonstrating the effectiveness of the current method in simulating flows which are largely parallel to the interface between the pure fluid and porous regions.

5.2. Porous Plug Flow

To validate the present method with regard to flows that are primarily perpendicular to the interface between the pure fluid and porous regions, the case of a steady plane channel with a porous plug, illustrated in Figure 6, was considered. This simple geometry is often used to determine experimentally the Darcy permeability K of a porous medium. Figure 7 presents the centerline velocity and pressure profiles

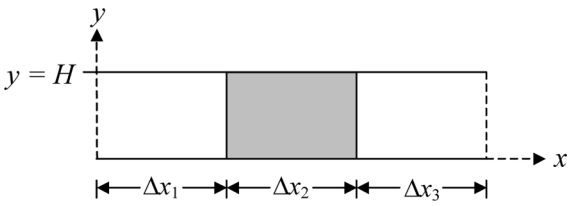

Figure 6. Geometry of porous plug test case for flow with a perpendicular interface.

for this case for Darcy numbers of 10^{-2} and 10^{-3}. The other parameters for the flows illustrated in Figure 7 were $\mathrm{Re}_H = 1$ and $\varepsilon = 0.7$, with the inertia coefficient c_E given by the same expression as in the previous case. The lengths illustrated in Figure 6 were set as $\Delta x_1 = \Delta x_3 = 3H$ and $\Delta x_2 = 2H$ for these cases. The boundary conditions set for the velocity profile were the usual fully developed profile for plane channel flow in a pure fluid at the inlet, i.e.,

$$u(0, y) = \frac{6Uy}{H}\left(1 - \frac{y}{H}\right) \qquad \text{and} \qquad v(0, y) = 0$$

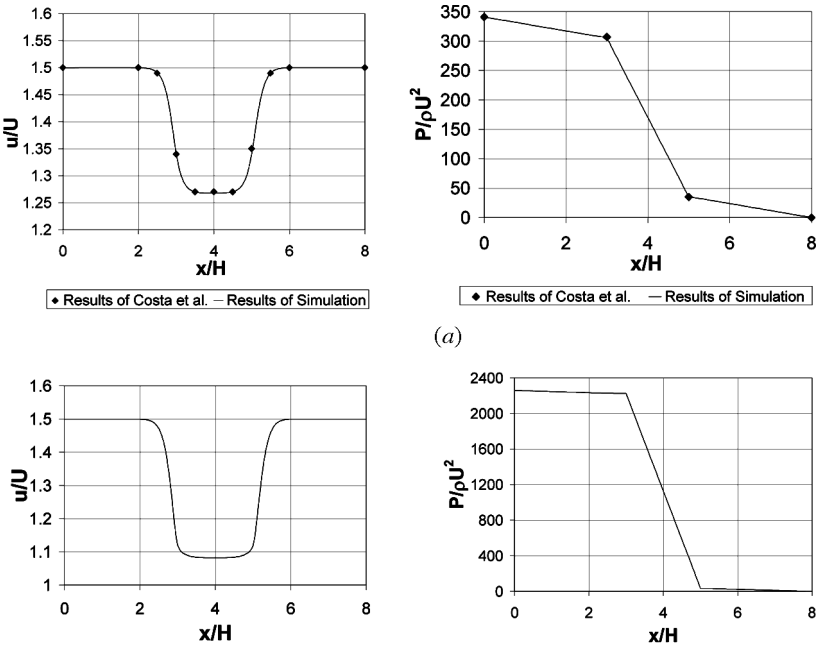

Figure 7. Centerline velocity and pressure profiles for porous plug problem with $\mathrm{Re} = 1$, $c_E = 1.75\varepsilon/(150\varepsilon^5)^{1/2}$, $\varepsilon = 0.7$, and (*a*) $\mathrm{Da} = 10^{-2}$, (*b*) $\mathrm{Da} = 10^{-3}$.

where U is the average axial velocity in the channel, zero derivative conditions in the x direction on both velocities at the outlet, and the typical conditions $u = v = 0$ at $y = 0$ and $y = H$. A uniform pressure condition was set at the outlet, and the pressure was extrapolated to all other boundaries. A nonuniform structured grid consisting of 21 control volumes in the y direction and 20 volumes in the x direction over each of Δx_1, Δx_2, and Δx_3, refined toward the interfaces and the boundaries at $y = 0$ and $y = H$, was found to give accurate results.

Examining Figure 7*a*, it is seen that the results of the present study are nearly identical to those of Costa et al. Clearly, the velocity profile reduces essentially to that for fully developed flow in pure fluid channel at relatively short distances on the pure fluid sides of the interfaces, as should be expected given the low Reynolds number, and to that for fully developed flow through porous medium at short distances inside the porous region. As expected from these observations, the pressure distribution is nearly linear in each of the three regions, and the pressure gradient may be seen to be discontinuous at the interfaces. Note that the pressure–velocity coupling remains strong at the interfaces under the present scheme. Figure 7*b* demonstrates similar behavior for the case of $\mathrm{Da} = 10^{-3}$, although as expected given the lower permeability, the velocity is more uniform across the height of the channel in the porous region, leading to a lower centerline velocity, and the flow reduces to the case of fully developed flow in porous media much more quickly. Note that although the results of the present study for $\mathrm{Da} = 10^{-3}$ are qualitatively similar to those of Costa et al., which are not shown here, there are some significant differences. For this case, Costa et al.'s results appear to show some relatively minor spurious oscillations in the velocity profile near the interface, which are absent in the present results. Also, Costa et al.'s results show a centerline velocity in the middle portion of the porous region of approximately 1.1 m/s, which is somewhat higher than the present results. However, the results computed here for the velocity distribution in the middle of the porous block match almost precisely the analytical solution of Vafai and Kim [23], giving credence to the present results since the flow appears to be essentially fully developed at that point.

To further demonstrate the effectiveness of the pressure–velocity coupling and the pressure estimate at the interface, one subsequent case was considered. In this case, the Darcy number was taken to be $\mathrm{Da} = 10^{-2}$, and the Reynolds number was set at $\mathrm{Re}_H = 1{,}000$, such that the dynamic pressure of the flow was $(1/2)\rho U^2 = 500$. For this case, the channel segment lengths indicated in Figure 6 were set at $\Delta x_1 = \Delta x_2 = 5H$ and $\Delta x_3 = 50H$, with the large value of Δx_3 chosen to ensure that the zero derivative condition could be specified at the outlet without affecting the flow in the region of interest. In all other regards, the conditions were the same as those described above. Figure 8 illustrates this flow for the range $x \in [0, 15H]$. The salient point of Figure 8 is that the velocity remains free of oscillations in the region near the interfaces at $x = 5H$ and $x = 10H$, indicating the effectiveness of the coupling and pressure estimate. Notice that due to the large dynamic pressure (high Re_H) and relatively low porosity, the dynamic corrections indicated by Eq. (43) are expected to be relatively large, and preliminary work by the authors indicated that a more simplistic pressure estimate, such as simple extrapolation, led to an unrealistic, oscillatory velocity profile. The current method is capable of dealing with flows such as this without introducing unphysical oscillations, while allowing for discontinuity in the pressure gradient at the interface.

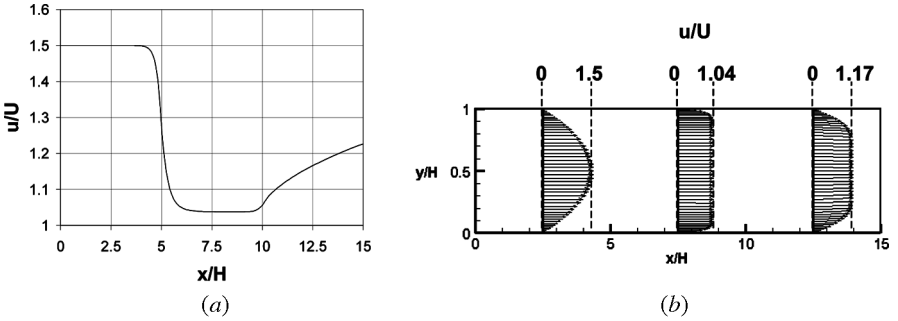

Figure 8. Streamwise velocity profile at (*a*) vertical centerline and (*b*) locations $x = 2.5H$, $x = 7.5H$, and $x = 12.5H$, for porous plug problem with $\mathrm{Re} = 1{,}000$, $1/2\rho U^2 = 500$, $\mathrm{Da} = 10^{-2}$, $c_E = 1.75\varepsilon/(150\varepsilon^5)^{1/2}$, and $\varepsilon = 0.7$.

5.3. Nonequilibrium Heat Transfer Problem

To test the nonequilibrium heat transfer model, the case considered by Calmidi and Mahajan [1] of steady, plane flow through an aluminum foam block heated from below was used. First, the simulation was carried out as suggested by Calmidi and Mahajan, simulating only the heated block and specifying the fully developed velocity profile of Vafai and Kim [23] at the inlet. This was done to verify the agreement of the authors' code with the results of Calmidi and Mahajan. Then, the simulation was run again, this time including the 2-mm air gap upstream of the heat block. Although the gap is small, it was felt that if the results of the simulation including the gap could be shown to be essentially equivalent to those without it, then it should be clear that the matching conditions for the energy equation are reasonable.

The simulations were run for Sample 2 of Calmidi and Mahajan [1]. The sample has a porosity $\varepsilon = 0.9118$, a ligament diameter $d_l = 0.55\,\mathrm{mm}$, a pore diameter $d_p = 3.80\,\mathrm{mm}$, an inertia coefficient $c_E = 0.085$, a permeability $K = 1.8 \times 10^{-7}\,\mathrm{m}^2$, a solid-phase effective conductivity $k_{\mathrm{se}} = 6.46\,\mathrm{W/m\,K}$, and a fluid-phase effect conductivity $k_{\mathrm{fe}} = 0.0237\,\mathrm{W/m\,K}$ for air flow. The fluid properties were taken to be those of air at 300 K. The interfacial heat transfer coefficient h_{sf} and the specific surface area A_{sf} were calculated in accordance with Calmidi and Mahajan, with the constant coefficient in the Nusselt number expression $\mathrm{Nu}_{sf} = h_{sf} d_l / k_f = C_T\,\mathrm{Re}_{d_l}^{0.5}\,\mathrm{Pr}^{0.37}$ set to $C_T = 0.52$. The dispersion conductivity was neglected. The block was taken to have a height of $H = 45\,\mathrm{mm}$ and a length in the flow direction of $L = 114\,\mathrm{mm}$. For the first case, simulating only the block, the fully developed profile velocity profile was set at the inlet as mentioned, with $u = v = 0$ specified at $y = 0$ and $y = H$, and zero derivative conditions in the x direction specified at the outlet. For the pressure distribution, a uniform pressure condition was specified at the outlet, and extrapolated conditions were specified at all other boundaries. The average streamwise velocity $U = 1.00\,\mathrm{m/s}$ was specified, and the experimental temperature distribution obtained by Calmidi and Mahajan for this condition was used at $y = 0$ to specify both the fluid and solid constituent temperature differences. The temperature difference is defined as $\theta_i = T_i - T_{\mathrm{in}}$, where in the porous region T_i may be $\langle T_f \rangle^f$, corresponding to θ_f, or $\langle T_s \rangle^s$, corresponding to θ_s. The temperature T_{in} is the

uniform inlet temperature. At the inlet, $\theta_f = 0$ was imposed by definition, while a zero normal gradient condition was imposed on the solid temperature profile to prevent back-conduction. Zero normal gradient conditions were imposed on both temperature profiles at the outlet, and at the adiabatic wall at $y = H$. For the case where the air gap was simulated, the same condition were imposed on the velocity and pressure distributions, and well as on the temperature distributions at the outlet and at $y = H$. At $y = 0$, the same conditions were imposed beneath the porous block, while an adiabatic condition was imposed at the bottom of the air gap. At the inlet, the condition $\theta_f = 0$ was imposed on the temperature distribution for the pure fluid region constituted by the air gap. For the first case, a grid of 70 control volumes in the y direction and 80 control volumes in the x direction, refined toward the boundaries at $y = 0$ and $y = H$, was found to produce an accurate result for the heat transfer rate per unit depth q'. For the second case, the same grid was used in the foam block, with some refinement toward the interface, and a section 7 volumes in width was used for the air-gap region.

Figure 9 gives the contour plots of the fluid and solid constituent temperature difference profiles, θ_f and θ_s. Figure 9*a* presents the case where the block alone is simulated, while Figure 9*b* gives the results for the simulation including the air gap. For the second plot of Figure 9*b*, note that θ_s is defined as zero in the pure fluid region. Clearly, the temperature profiles within the porous region are essentially identical in both cases. In this case, it can be seen that the effects on thermal nonequilibrium are not particularly strong throughout the majority of the flow. However, at higher velocities or, of pertinence to the authors' work, in the case were the solid-phase effective conductivity is considerably greater, the effects of

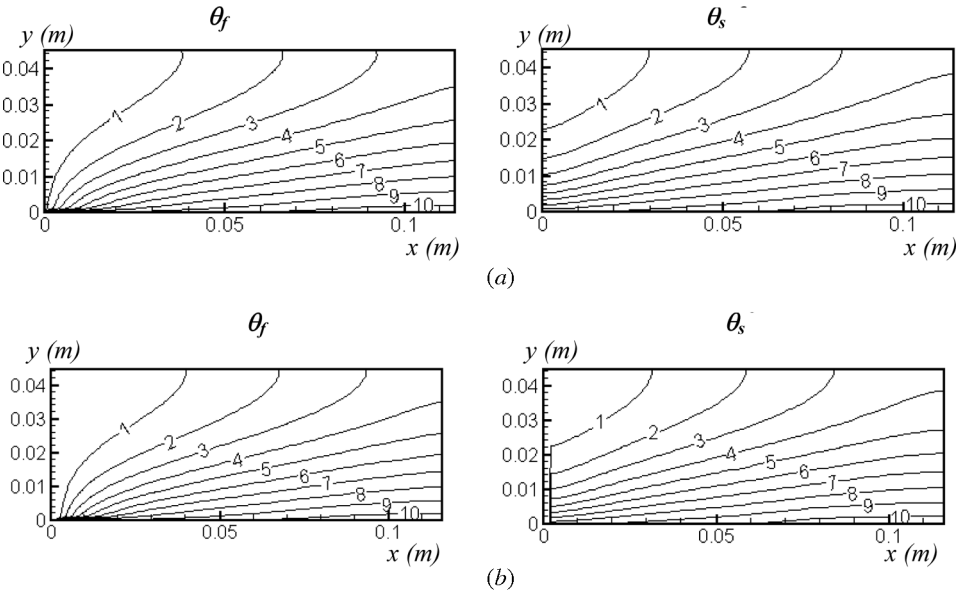

Figure 9. Temperature difference distributions θ_f and θ_s for heated block test case, simulating (*a*) block only, and (*b*) block and air gap.

nonequilibrium should become more evident. In that case, neglecting the nonequilibrium effects is expected to result in unacceptable errors. In both simulations, the heat transfer rate per unit depth was found to be $q' = 315\,\mathrm{W/m}$. This leads to an overall Nusselt number, defined by $\mathrm{Nu} = \overline{h}L/k_{\mathrm{eff}} = q'/k_{\mathrm{eff}}\,\Delta T_{\mathrm{avg}}$, of $\mathrm{Nu} \approx 5.1$, where ΔT_{avg} is the difference between the average temperature at $y = 0$ and T_{in}. This is in excellent agreement with the result presented by Calmidi and Mahajan for the relevant parameters $\mathrm{Re}_K = 26.7$ and $\mathrm{Pr}_{\mathrm{eff}} = 2.88 \times 10^{-3}$.

6. CONCLUSIONS

A mathematical and numerical model for the treatment of conjugate fluid flow and heat transfer problems in domains containing pure fluid, porous, and pure solid regions has been presented. The model is general and physically reasoned, and allows for local thermal nonequilibrium in the porous region. Rigorous validation has demonstrated the ability of the model to provide accurate solutions to a variety of problems.

REFERENCES

1. V. V. Calmidi and R. L. Mahajan, Forced Convection in High Porosity Metal Foams, *J. Heat Transfer*, vol. 122, pp. 557–565, 2000.
2. M. S. Phanikumar and R. L. Mahajan, Non-Darcy Natural Convection in High Porosity Metal Foams, *Int. J. Heat Mass Transfer*, vol. 45, pp. 3781–3793, 2002.
3. G. Beavers and D. D. Joseph, Boundary Conditions at a Naturally Permeable Wall, *J. Fluid Mech.*, vol. 30, pp. 197–207, 1967.
4. B. Alazmi and K. Vafai, Analysis of Fluid Flow and Heat Transfer Interfacial Conditions between a Porous Medium and a Fluid Layer, *Int. J. Heat Mass Transfer*, vol. 44, pp. 1735–1749, 2001.
5. B. Alazmi and K. Vafai, Analysis of Variants within the Porous Media Transport Models, *J. Heat Transfer*, vol. 122, pp. 303–326, 2000.
6. M. L. Martins-Costa and R. M. Saldanha de Gama, A Local Model for the Heat Transfer Process in Two Distinct Flow Regions, *Int. J. Heat Fluid Flow*, vol. 15, pp. 477–485, 1994.
7. S. Chikh, A. Boumedien, K. Bouhadef, and G. Lauriat, Analysis of Fluid Flow and Heat Transfer in a Channel with Intermittent Heated Porous Blocks, *Heat Mass Transfer*, vol. 33, pp. 405–413, 1998.
8. W. S. Fu and S. F. Chen, A Numerical Study of Heat Transfer of a Porous Block with the Random Porosity Model in a Channel Flow, *Heat Mass Transfer*, vol. 38, pp. 695–704, 2002.
9. Y. Ould-Amer, S. Chikh, K. Bouhadef, and G. Lauriat, Forced Convection Cooling Enhancement by Use of Porous Materials, *Int. J. Heat Fluid Flow*, vol. 19, pp. 251–258, 1998.
10. V. A. F. Costa, L. A. Oliveira, B. R. Baliga, and A. C. M. Sousa, Simulation of Coupled Flows in Adjacent Viscous and Porous Domains Using a Control-Volume Finite-Element Method, *Numer. Heat Transfer A*, vol. 45, pp. 675–697, 2004.
11. M. Kaviany, *Principles of Heat Transfer in Porous Media*, 2nd ed., Springer-Verlag, New York, 1995.
12. S. Whittaker, Volume Averaging of Transport Equations, in J. Prieur du Plessis (ed.), *Fluid Transport in Porous Media*, chap. 1, Computational Mechanics Publications, Southampton, UK, 1997.

13. K. Vafai and C. L. Tien, Boundary and Inertia Effects on Flow and Heat Transfer in Porous Media, *Int. J. Heat Mass Transfer*, vol. 24, pp. 195–203, 1981.
14. A. Amiri, K. Vafai, and T. M. Kuzay, Effects of Boundary Conditions on Non-Darcian Heat Transfer through Porous Media and Experimental Comparisons, *Numer. Heat Transfer A*, vol. 27, pp. 651–664, 1995.
15. D. K. Gartling, C. E. Hickox, and R. C. Givler, Simulation of Coupled Viscous and Porous Flow Problems, *Comput. Fluid Dynam.*, vol. 7, pp. 23–48, 1996.
16. K. Vafai and R. Thiyagaraja, Analysis of Flow and Heat Transfer at the Interface Region of a Porous Medium, *Int. J. Heat Mass Transfer*, vol. 30, pp. 1391–1405, 1987.
17. J. A. Ochoa-Tapia and S. Whitaker, Momentum Transfer at the Boundary between a Porous Medium and a Homogeneous Fluid—I. Theoretical Development, *Int. J. Heat Mass Transfer*, vol. 38, pp. 2635–2646, 1995.
18. W. O. Williams, Constitutive Equations for Flow of an Incompressible Viscous Fluid through a Porous Medium, *Q. Appl. Math.*, vol. 36, pp. 255–267, 1978.
19. K. Vafai and S. J. Kim, On the Limitations of the Brinkman-Forchheimer-Extended Darcy Equation, *Int. J. Heat Fluid Flow*, vol. 16, pp. 11–15, 1995.
20. S. V. Patankar, *Numerical Heat Transfer and Fluid Flow*, Hemisphere, Washington, DC, 1980.
21. C. M. Rhie and W. L. Chow, Numerical Study of the Turbulent Flow past an Airfoil with Trailing Edge Separation, *AIAA J.*, vol. 21, pp. 1525–1532, 1983.
22. B. Alazmi and K. Vafai, Constant Wall Heat Flux Boundary Conditions in Porous Media under Local Thermal Non-equilibrium Conditions, *Int. J. Heat Mass Transfer*, vol. 45, pp. 3071–3087, 2002.
23. K. Vafai and S. J. Kim, Forced Convection in a Channel Filled with a Porous Medium: An Exact Solution, *J. Heat Transfer*, vol. 111, pp. 1103–1106, 1989.